

Original Research

Association of Retinal Nerve Fiber Layer Thickness with Brain Microstructural Changes in Participants with White Matter Hyperintensities

Yucong Wu^{1,†}, Jueyue Yan^{2,†}, Lu Xu¹, Chunfei Xu¹, Meiqi Zhao¹, Zhenxiang Zhan¹, Yi Lu³, Xiaozhen Liu⁴, Yungang Cao^{1,*}, Zhao Han^{1,*}¹Department of Neurology, The Second Affiliated Hospital and Yuying Children's Hospital of Wenzhou Medical University, 325027 Wenzhou, Zhejiang, China²Critical Care Medicine, The First Affiliated Hospital, Zhejiang University School of Medicine, 310003 Hangzhou, Zhejiang, China³Department of Radiology, The Second Affiliated Hospital and Yuying Children's Hospital of Wenzhou Medical University, 325027 Wenzhou, Zhejiang, China⁴China-USA Neuroimaging Research Institute, Department of Radiology of the Second Affiliated Hospital and Yuying Children's Hospital, Wenzhou Medical University, 325027 Wenzhou, Zhejiang, China*Correspondence: caoyungang2003@163.com (Yungang Cao); wzhanzhao@aliyun.com (Zhao Han)

†These authors contributed equally.

Academic Editor: Gernot Riedel

Submitted: 19 August 2023 Revised: 20 October 2023 Accepted: 25 October 2023 Published: 11 March 2024

Abstract

Purpose: White matter hyperintensity (WMH) is suggested to cause stroke and dementia in older adults. Retinal structural thicknesses revealed by optical coherence tomography (OCT) are associated with structural changes in the brain. We aimed to explore the association between the peripapillary retinal nerve fiber layer (RNFL) and cerebral microstructural changes in participants with white matter hyperintensities (WMH). **Methods:** Seventy-four participants (37 controls, healthy control (HC), and 37 older adults with WMH) underwent retinal and brain imaging using OCT and magnetic resonance imaging (MRI) respectively. Peripapillary RNFL thickness was assessed by the OCT. Gray matter volume (GMV) was assessed from a T1-weighted MRI. White matter integrity was assessed with diffusion tensor imaging (DTI) while WMH severity was assessed with the Fazekas scale. All participants underwent a neuropsychological examination (Mini-Mental State Examination, MMSE). **Results:** Older adults with WMH showed thinner peripapillary RNFL ($p = 0.004$) thickness when compared with the control group after adjusting for age, hypertension and gender. In our older adults with WMH, RNFL thickness correlated with fractional anisotropy (FA) in the superior longitudinal fasciculus (SLF) ($\text{Rho} = -0.331, p < 0.001$). In older adults with WMH, RNFL was significantly associated with MMSE scores ($\text{Rho} = 0.422, p < 0.001$) and Fazekas scores ($\text{Rho} = -0.381, p = 0.022$) respectively. **Conclusions:** We suggest neurodegeneration of peripapillary RNFL in older adults with WMH was associated with cerebral microstructural volume, impaired cerebral axonal damage, and cognitive performances. OCT metrics may provide evidence of neurodegeneration that may underpin WMH and cerebral microstructural changes in the brain. **Clinical Trial Registration:** This study was registered online at the China Clinical Trial Registration Center (registration number: ChiCTR-ROC-17011819).

Keywords: white matter hyperintensity; optical coherence tomography; peripapillary retinal nerve fiber layer; diffusion tensor imaging; cognition

1. Introduction

White matter hyperintensity (WMH) of presumed vascular origin is a major cause of stroke and dementia in the aging population [1,2], however, its underlying mechanism remains unclear and treatments are limited. Recent reports [1,3] suggested that WMH is associated with cerebral vascular impairment. WMH is a feature of cerebral small vessel disease (SVD) and is common in older adults. WMH can be seen on magnetic resonance imaging (MRI) scans as hyperintense on T2-weighted scans.

The retina and the brain share many features such as embryologic origin, precise neuronal cell layers, blood barriers, and microvasculature [4]. As opposed to the brain, the retina is directly visible using standard ophthalmology

tools. Since the retina is visible and shares a similar neurobiology with the brain, it can be used to develop a point-of-care test that can detect disease-related biomarkers at an early stage. It has been reported that subtle alterations in the retina may reflect the pathological changes of the brain during a disease cascade [5]. The retinal nerve fiber layer (RNFL) has been reported to be a useful structural biomarker for neurodegeneration in the eye [6]. Optical imaging modalities such as spectral-domain optical coherence tomography (SD-OCT) provide a non-invasive *in vivo* visualization and quantification of the RNFL thickness.

Previous reports have shown significant macula thinning in patients with WMH [7], dementia [8], and mild cognitive impairment when compared with healthy controls. A



previous report with a large sample size showed that thinning of the RNFL is associated with a higher risk of increasing dementia and proposed that alterations in the RNFL may be a structural biomarker for dementia [9–12]. Ong *et al.* [13] recruited elderly adults without dementia and found an association between the changes in the RNFL thickness and changes in the mediotemporal lobe volumes. Cerebral imaging modalities such as diffusion tensor imaging (DTI) has been reported to be a good imaging technique for the evaluation of white matter integrity of the brain [14,15]; it is also sensitive to global age-related changes that occur in the brain and may be useful in the retinal changes as well.

Here, we investigated the associations between retinal thickness measured using OCT and microstructural volume measures from brain MRI and DTI measurements of white matter microstructural integrity in older adults with WMH.

2. Materials and Methods

Older adults who were ≥ 50 years old were enrolled in our study and underwent cerebral MRI and ophthalmological examinations as shown in **Supplementary Fig. 1**. Older adults with WMH were included in our study based on the presence of WMH on MRI scans. We excluded participants with contraindications to MRI or incapacity to consent. Assessments included clinical, lifestyle, blood tests, brain and retinal imaging. The rationale for the study along with the protocol and design of this study have been well documented in our previous study [16].

Older adults (≥ 50 years old) who attended our hospital but did not show any neurologic disorder on magnetic resonance (MR) imaging were enrolled in our study as controls. Individuals were excluded from the study if they had the following: toxic disorders affecting the central nervous system (CNS), history of substance abuse, and medical ailment involving the use of concomitant corticosteroid or immunosuppressant therapy. Lifestyle and clinical information were recorded for all controls.

This study was approved by the Ethics Committee of the Second Affiliated Hospital and Yuying Children's Hospital of Wenzhou Medical University (Ethics Approval No. 10 [2017], Clinical Science Review) and all participants gave written informed consent. All procedures in this study followed the Declaration of Helsinki.

Clinical information such as hypertension, diabetes mellitus, hyperlipidemia, smoking, and alcohol were recorded. Resting blood pressure measurements were also done for all participants. All participants underwent neuropsychological tests before MR imaging and OCT imaging. Mini-Mental State Examination, which is a dementia screening tool with a total score of 30; a higher score represents better cognition.

2.1 MRI Brain Imaging

Full details of the brain imaging scanning protocol have been published [16]. Briefly, a Siemens 3 Tesla Trio

MRI scanner (Signa HDxt GE Healthcare, Milwaukee, WI, USA) equipped with a 32-channel head coil was used for all imaging; a standardized protocol was used in all patients including T1-weighted images, T2-weighted images, and fluid-attenuated inversion recovery (FLAIR) imaging. WMH was evaluated on FLAIR images using the Fazekas scale [17]. WMH severity was rated (0–3) separately for deep and periventricular regions of the brain, with the sum of the scores representing the total WMH burden as shown in Fig. 1.

2.2 FSL-VBM

Image processing for calculating brain gray matter volume based on voxel-based morphometry (VBM). The voxel-based morphological determination is carried out by using the FSL-VBM software package (Analysis Group, FMRIB, Oxford, UK), and all imaging images are processed in the default standard mode as follows: (1) The graphic format is changed by MRICRO software (<https://www.nitrc.org/projects/mricron/>, Analysis Group, FMRIB, Oxford, UK) to convert the digital imaging and communications in medicine (DICOM) data of 3DT1 images into NII format, so that they can be recognized and processed by fmrib software library (FSL), and the tissues with artifacts are removed manually. (2) Use the brain extraction (BET) toolkit of FSL software to remove the skull of all the included brain magnetic resonance images, and manually screen the processed images. If they do not reach the standard, adjust the corresponding parameters in the BET software (Analysis Group, FMRIB, Oxford, UK), and repeat the above steps until the ideal image is obtained. (3) Using the fully automatic recognition and cutting tool tissue type segmentation (FAST4) in FSL, the image obtained in step 2 is segmented and divided into gray matter, cerebrospinal fluid, white matter and other tissues. Using linear registration (FLIRT) tool (Analysis Group, FMRIB, Oxford, UK), the recognized gray matter image and its mirror data are registered to the standard Montreal Neurological Institute (MNI) template of FSL, and the gray matter image and mirror image registered to the standard template are automatically synthesized into a 4D image. A template based on this study [spatial resolution ($2 \times 2 \times 2$) mm³] is obtained by averaging all gray matter images in the 4D image. (4) The nonlinear registration tool non-linear registration (FNIRT) is used to map the image processed in step 1 to the template generated by step 3. Due to the replication of the registration process. It is easy to be affected by the magnetic field, which leads to the image becoming smaller, shrinking or expanding. FSL-VBM also introduces the calibration function, which divides each pixel value in the image by the value of the Jacobian determinant of the deformation field, and then automatically connects the corrected gray matter image to generate a new standard image, and uses a filter with Gaussian kernel to smooth it spatially.

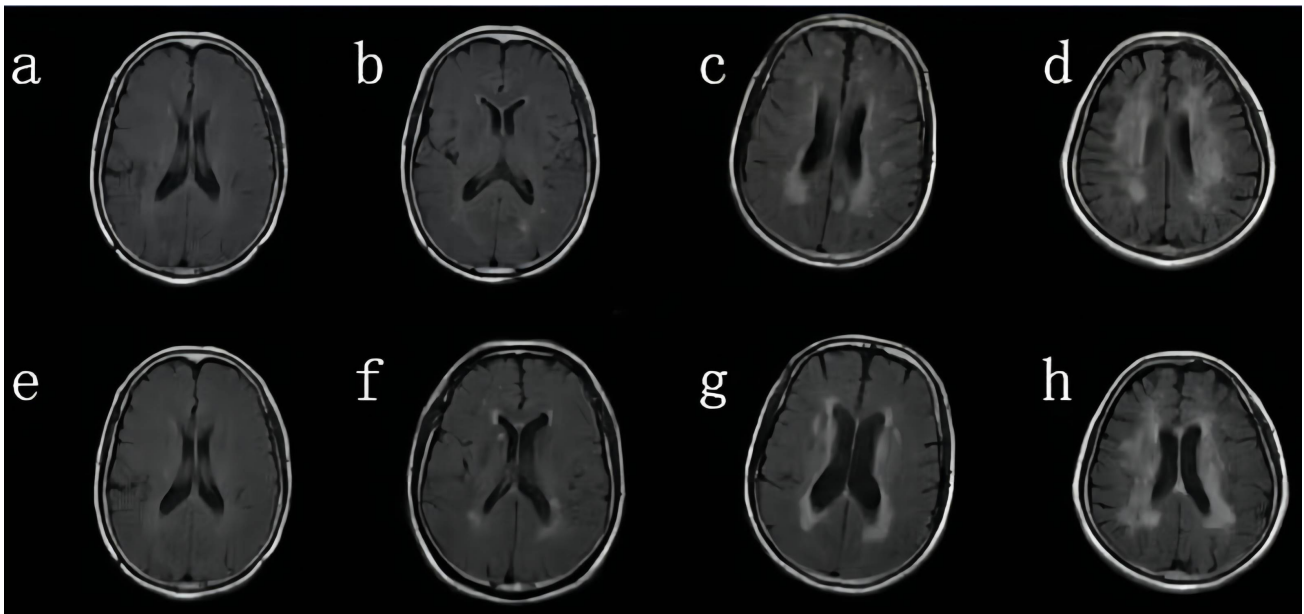


Fig. 1. Visual rating of white matter hyperintensities (WMH) using the Fazekas scale. (a–d) Subcortical deep white matter hyperintensity—0 score: no lesion (a); 1 score: punctate lesion (b); 2 scores: lesion fusion (c); 3 scores: large area fusion of lesion (d); (e–h) paraventricular WMH—0 score: no lesion (e); 1 score: pencil or false thin layer lesion (f); 2 scores: smooth halo (g). 3 scores: irregular paraventricular high signal intensity extending to the deep white matter (h); the lesion scores of the two sites were added (minimum 0 scores, maximum 6 scores).

2.3 Processing of the DTI Images Was Done Using the FSL Package

Diffusion imaging was used to assess white matter integrity in our study participants. Image analysis is carried out by the process of tract-based spatial statistics (TBSS) in FSL software. Data were inspected for movement artifacts using FSL-MCFLIRT (<https://fsl.fmrib.ox.ac.uk/fsl/fslwiki/MCFLIRT>) ($<1^\circ$ rotation and <1 mm translation) and then corrected for eddy current-induced distortions. FSL was used to perform the brain extraction and calculation of diffusion parameter maps. Fractional anisotropy (FA) maps for each participant were registered into a standard brain template (FMRIB58 FA, part of the FSL suite) using the nonlinear spatial transformation tool FNIRT. A mean FA image was then compiled by averaging aligned FA maps from each participant. To generate a mean FA skeleton representing the centers of all tracts common to the group, the map threshold was then set for voxels showing FA values ≥ 0.2 . Aligned FA maps for each participant were projected onto the standard skeletonized FA image (FMRIB58 FA-skeleton, packaged in FSL) by searching the area around the skeleton in the direction perpendicular to each tract, finding the highest local FA value, and assigning this value to the skeleton [18].

VBM and TBSS are both whole-brain comparisons. We locate gray matter differential brain regions based on the anatomical automatic labeling 3 (AAL3) brain template [19]. We position white matter fiber bundles based on the international consortium for brain mapping-diffusion

tensor imaging (ICBM-DTI-81) white-matter labels atlas (<https://cmrm.med.jhmi.edu/>) [20]. We then extracted signals from different brain regions for further analysis. During processing, the average map is produced to register into a standard MNI152 space.

Participants also underwent fundus and optic disc imaging using fundus photography. Abnormalities of the optic disc and macular were defined as present if any of the following were detected: retinal and/or optic nerve head hemorrhage, soft and hard exudates, retinal and/or optic disc edema, papilledema and optic disc atrophy. If a participant presented with any of these abnormalities, the participant was excluded from our study.

2.4 Spectral Domain Optical Coherence Tomography (SD-OCT)

The Avanti RTVue-XR (software version 2017.100.0.1, Optovue, Fremont, CA, USA) was used to image the retinal structure for all participants. The imaging tool has a scan speed of 100 KHz, a wavelength of 840 nm with a tuning range of 100 nm. The image resolution was 5.3 mm axially and 18 mm laterally. In our study, the mean peripapillary retinal nerve fiber layer (RNFL) was automatically generated by the optical coherence tomography (OCT) tool. The RNFL thickness was acquired using the optic nerve head (ONH) map protocol, with a scanning range covering a diameter of 3.45 mm centered on the optic disc as shown in Fig. 2. OCT images with ophthalmic disorders such as age-macular

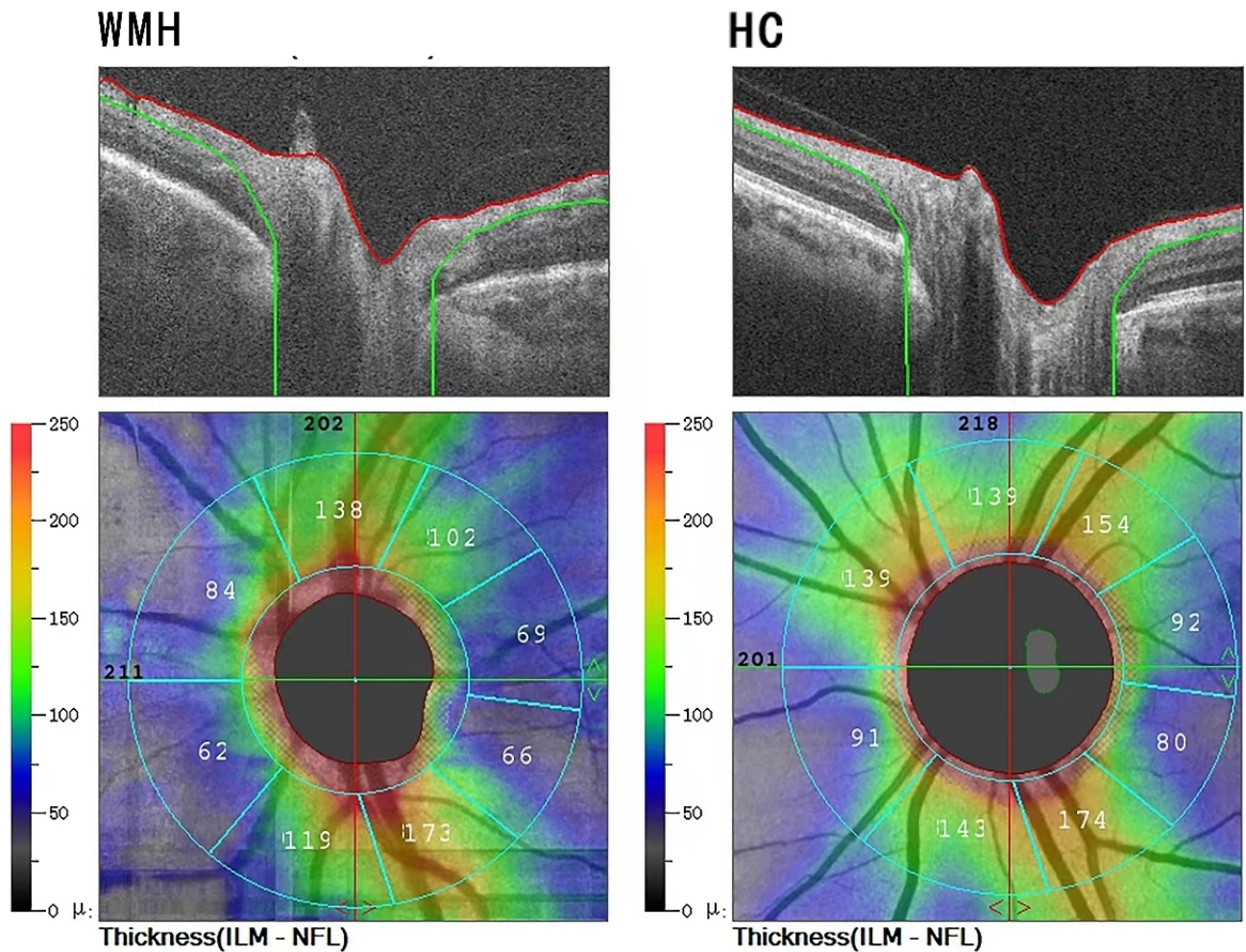


Fig. 2. Segmentation of optical coherence tomography (OCT) images. The upper row represents the Spectral domain optical coherence tomography (SD-OCT) tomographic images; the system automatically recognizes the peripapillary retinal nerve fiber layer (pRNFL) and calculates its thickness, using color to represent the thickness, cool color (green) represents thinner pRNFL thickness, and warm color (red) represents thicker thickness. The lower row represents the retina SD-OCT image; The retina SD-OCT image is automatically extracted to calculate the pRNFL thickness. The left is the representative picture of the WMH group, and the right is the healthy control group (HC). ILM-NFL, Inner limiting membrane-Nerve fiber layer.

degeneration, severe cataracts, optic neuritis, diabetic retinopathy, glaucoma, and optic neuritis were excluded. If a participant presented with any of these disorders in one eye, the other eye was used; if both eyes had the disorders aforementioned, the participant was excluded from the study. OCT images with a signal quality of less than 7 were excluded from our study. OCT data displayed in our study followed the OSCAR-IB quality criteria [21] and the Advised Protocol for OCT Study Terminology and Elements (APOSTEL) recommendation [22].

2.5 Statistical Analyses

The normality of data was done by visual inspection of the distribution and Kolmogorov-Smirnov test. Consecutive variables with normal distribution were expressed as mean and standard deviation (SD). Categorical variables are presented as frequencies and percentages (%).

2.5.1 FSL-VBM

Non-parametric statistical analyses “Randomize” were used to compare differences in grey matter volume between the two groups. Multiple comparisons correction was performed using threshold-free cluster enhancement (TFCE) option with 5000 permutations. $p < 0.05$ was considered that the difference was statistically significant.

2.5.2 Diffusion Tensor Imaging (DTI)

Using tract-based spatial statistics tools, a voxel-wise spatial statistical analysis comparing both groups was performed using a ‘randomized’ program within FSL, which involves permutation testing [18]. The mean FA skeleton was used as a mask (threshold at a mean FA value of 0.2), and the number of permutations was set to 5000. Thresholding was performed using threshold-free cluster enhancement, a new method for finding significant clusters in MRI

data without having to define them as binary units [23]. Clusters were assessed for multiple comparisons using the family-wise error rate ($p < 0.05$).

2.5.3 Optical Coherence Tomography (OCT)

An eye of each participant was included in the data analyses. In cases where both eyes met the criteria, the eye was selected according to the higher signal strength index of the macular in the OCT-A imaging; when the signal strength index (SSI) of OCT-A images was the same in both eyes, the quality of ONH images was decisive. Multiple linear regression models using generalized estimation equations (GEE) were done to analyze changes that occur in WMH and healthy control (HC) and associations between the RNFL and cerebral parameters. The models were adjusted for signal strength index (SSI), age, hypertension, eye used (whether left or right), and sex. p values less than 0.05 were considered statistically significant. All statistical analyses were performed using SPSS version 21 (IBM Corp., Armonk, NY, USA).

3. Results

We identified 43 older adults with WMH and 45 older adults without WMH as controls. Participants were excluded because of either poor MRI scans, macular pathologic findings, or poor-quality OCT scans as shown in **Supplementary Fig. 1**. Table 1 displays the characteristics of our study participants. Thirty-seven WMH participants (mean age = 66.19 years) and 37 controls (mean age = 64.91 years) were included in the data analyses. Significant changes ($p > 0.05$) were not seen in sex, age, body mass index (BMI), blood pressure (including systolic blood pressure, diastolic blood pressure, mean arterial pressure), vascular risk factors (including smoking, alcohol, hypercholesterolemia), blood biochemical indexes [including hemoglobin A1c (HbA1c), triglycerides (TG), total cholesterol (TC), low-density lipoprotein cholesterol (LDL-c), high-density lipoprotein cholesterol (HDL-c), homocysteine (Hcy), serum creatinine (Scr)], visual acuity and intraocular pressure. Moreover, older adults with WMH had increased Fazekas scores ($p < 0.001$), worse Mini-Mental State Examination (MMSE) scores ($p < 0.001$) and thinner peripapillary retinal nerve fiber layer (pRNFL) thickness ($p = 0.004$) compared to the control group as shown in Table 1.

Table 2 and Fig. 3 show the comparison of cerebral microstructural volume between the groups. Older adults with WMH showed significantly reduced gray matter volume (GMV) in the left frontal inferior orbital gyrus ($p = 0.014$), left superior temporal gyrus ($p = 0.04$), left frontal middle orbital gyrus ($p = 0.013$), left cerebellum ($p < 0.001$), left inferior temporal gyrus ($p = 0.007$) when compared to the control group.

Compared to the control group, older adults with WMH had lower FA in the superior longitudinal fasciculus (SLF) ($p = 0.027$) and splenium of corpus callosum ($p < 0.001$) as shown in Table 3 and Fig. 4.

Table 1. Characteristics of study participants.

	WMH	Controls	p value
	(n = 37)	(n = 37)	
Gender, males	22 (59.5%)	24 (64.8%)	0.716
Age, years	66.19 ± 7.52	64.91 ± 4.03	0.358
Education, years	7.01 ± 2.02	7.95 ± 1.93	0.855
Smokers, n (%)	12 (32.4%)	14 (37.8%)	0.377
Drinkers, n (%)	5 (13.5%)	6 (16.2%)	0.821
Hypertension, n (%)	12 (32.4%)	10 (27.0%)	0.376
Diabetes mellitus, n (%)	3 (8.10%)	2 (5.40%)	0.887
BMI, kg/m ²	23.94 ± 3.50	22.58 ± 2.70	0.812
SBP, mmHg	135.51 ± 12.29	133.41 ± 14.36	0.849
DBP, mmHg	78.75 ± 9.15	76.54 ± 9.02	0.784
MAP, mmHg	95.12 ± 8.72	94.32 ± 9.77	0.910
Fazekas score	3.70 ± 1.41	1.0 ± 0.52	<0.001
MMSE score	21.09 ± 3.91	26.30 ± 3.13	<0.001
HbA1c, %	6.61 ± 1.02	6.01 ± 1.10	0.901
TG, mmol/L	1.42 ± 0.44	1.20 ± 0.25	0.090
TC, mmol/L	4.81 ± 0.55	4.25 ± 0.45	0.558
LDL-c, mmol/L	2.65 ± 0.74	2.22 ± 0.66	0.685
HDL-c, mmol/L	1.42 ± 0.58	1.56 ± 0.64	0.758
Hcy, μmol/L	12.33 ± 3.32	10.08 ± 1.77	0.772
Scr, μmol/L	77.25 ± 14.52	82.45 ± 15.02	0.651
SE, D	0.53 ± 2.26	0.63 ± 1.90	0.950
IOP, mmHg	12.51 ± 2.91	11.64 ± 3.26	0.782
BCVA	0.97 ± 0.20	1.04 ± 0.14	0.071
AL, mm	23.38 ± 0.80	22.98 ± 0.83	0.985
pRNFL, μm	110.0 ± 11.09	116.92 ± 8.48	0.004*

BMI, body mass index; SBP, systolic blood pressure; DBP, diastolic blood pressure; MAP, mean arterial pressure; MMSE, Mini-Mental State Examination; HbA1c, hemoglobin A1c; TG, triglycerides; TC, total cholesterol; LDL-c, low-density lipoprotein cholesterol; HDL-c, high-density lipoprotein cholesterol; Hcy, homocysteine; Scr, serum creatinine; SE, spherical error; IOP, intraocular pressure; BCVA, best corrected visual acuity; AL, axial length; pRNFL, peripapillary retinal nerve fiber layer.

* p value was adjusted for age, gender, hypertension, signal quality of retinal image and eye used.

In older adults with WMH, RNFL thickness correlated with GMV in the left frontal inferior orbital gyrus ($Rho = -0.506$, $p = 0.002$) and left frontal middle orbital gyrus ($Rho = -0.424$, $p = 0.010$).

In our older adults with WMH, RNFL thickness correlated with FA changes in the SLF ($Rho = -0.331$, $p < 0.001$; Fig. 5A); no significant correlation ($p > 0.05$) was seen between RNFL thicknesses and other DTI parameters in our study cohort.

In older adults with WMH, RNFL was significantly associated with MMSE scores ($Rho = 0.422$, $p < 0.001$; Fig. 5B) and Fazekas scores ($Rho = -0.381$, $p = 0.022$) respectively. In older adults without WMH, no significant correlation was seen between RNFL thickness and MRI parameters ($p > 0.05$, data not shown).

Table 2. Comparison of GMV parameters between older adults with WMH group compared with the control group.

Region	Ba	Cluster size, mm ³	MNI coordinates		
			x	y	z
L frontal inferior orbital gyrus	47	116	-38	34	-6
L superior temporal gyrus	48	135	-48	-36	24
L frontal middle orbital gyrus	11	242	-32	38	-20
L cerebellum		295	-22	-58	-62
L inferior temporal gyrus	20	4509	-46	2	-38

MNI, Montreal Neurological Institute; Ba, Brodmann area; GMV, gray matter volume.

Table 3. Comparison of fractional anisotropy (FA) parameters between older adults with WMH group compared with the control group.

Region	Region size (voxels)	MNI coordinates		
		x	y	z
Superior longitudinal fasciculus	29	-38	-25	45
Splenium of corpus callosum	98	14	-46	10

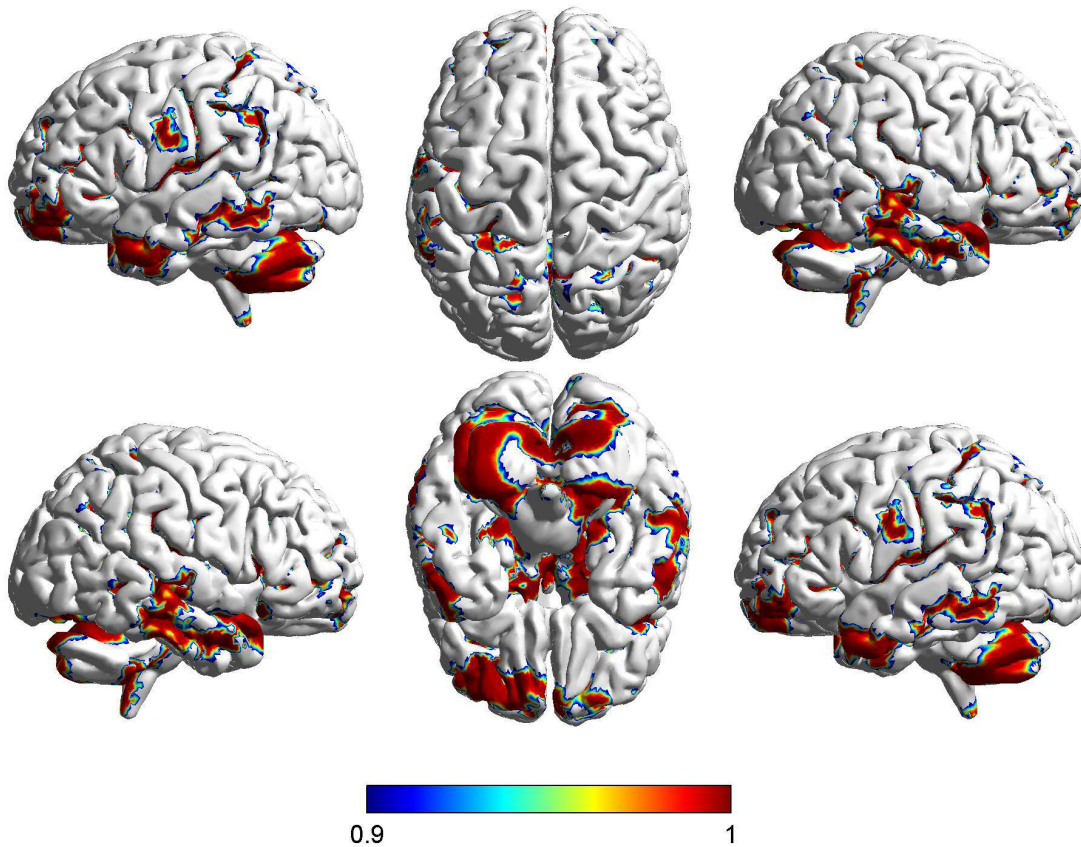


Fig. 3. Difference in cortical volume between WMH and healthy controls. FSL-voxel-based morphometry (VBM) showed brain regions with differences in cortical volume in the WMH group compared with the control group, which was demonstrated by the Montreal Institute of Neurology model. The cortical volume of WMH group became smaller, which was indicated by red. The brain regions that show differences in cortical volume between the WMH group and the control group are as follows: left frontal inferior orbital gyrus, left superior temporal gyrus, left frontal middle orbital gyrus, left cerebellum, left inferior temporal gyrus. The value of the colour bar indicates 1-P. The red colour indicates the direction in which the difference between the two groups is large, while the blue colour indicates the direction in which the difference between the two groups is relatively small. $p < 0.05$, threshold-free cluster enhancement (TFCE) correction.

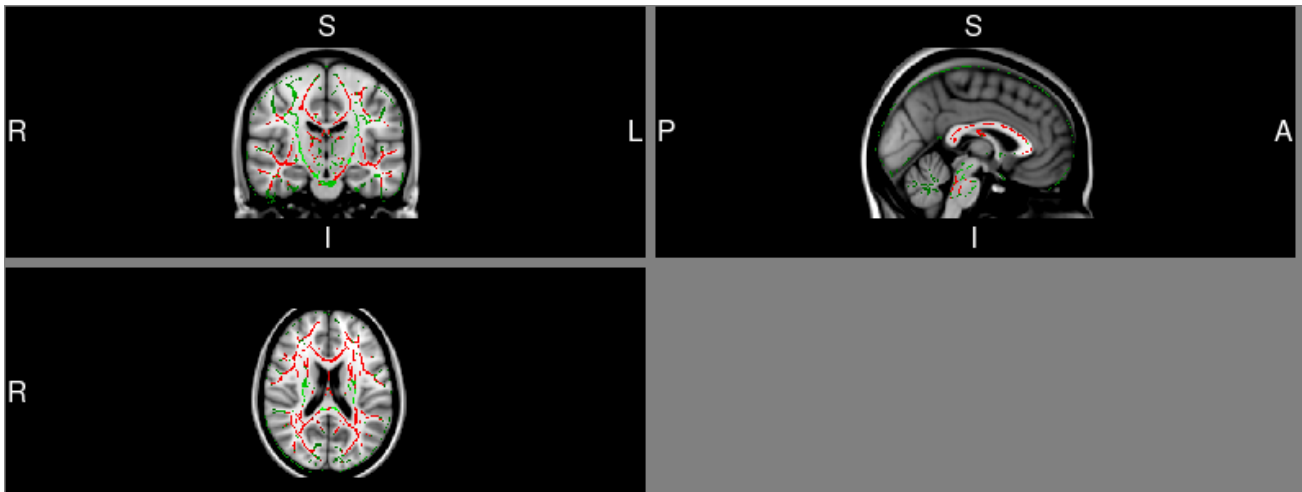


Fig. 4. Difference in fractional anisotropy (FA) values between WMH and healthy controls. WMH participants shown significantly reduced FA values in superior longitudinal fasciculus (SLF), and splenium of corpus callosum when compared to healthy control (HCs). Green is the standard whole-brain fibre skeleton, and red indicates fibre bundles that are significantly different between the two groups. $p < 0.05$, TFCE correction.

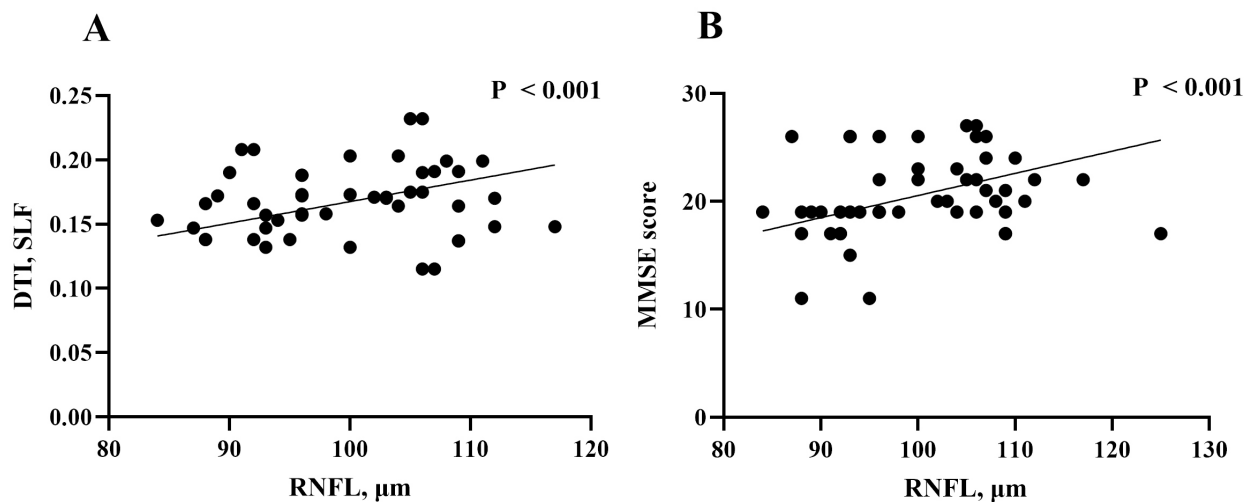


Fig. 5. The relationship of DTI variables, clinical parameters and RNFL thickness in WMH participants. (A) Correlation of retinal nerve fiber layer (RNFL) thickness and DTI variables in WMH participants. (B) Correlation of RNFL thickness and clinical parameters in WMH participants.

4. Discussion

This observational study demonstrates that thinner RNFL thickness in older adults with WMH was associated with reduced GMV and FA parameters. We also showed that thinner RNFL thickness in older adults with WMH correlated with increased Fazekas scores and lower montreal cognitive assessment (MoCA) scores.

Previous studies [12,16,24,25] showed WMH participants have thinner RNFL thickness compared to controls and suggested that the thinning of the RNFL may be due to transneuronal retrograde degeneration. Here we showed the peripapillary RNFL thickness was thinner in older adults with WMH when compared to controls. The peripapillary

RNFL is located around the optic nerve head and is mainly composed of ganglion cell axons [5,13]. Besides, it is suggested that this retinal parameter is sensitive to white matter microstructural changes in the brain [5,26]. Here, we suggest that changes in the peripapillary RNFL may reflect the axonal damage (neurodegeneration) occurring in the brain.

Accumulating studies [26–28] have shown that retinal structural changes are associated with white matter microstructural changes, yet how these structural changes are related to other brain parameters is underexplored. We showed that in older adults with WMH, the GMV of the left superior temporal gyrus and inferior temporal gyrus was reduced when compared with the control group. The Wernick area is behind the left superior temporal gyrus and is

responsible for language understanding. These structural changes may be the anatomical basis of cognitive function changes in patients with WMH. Besides, we showed that the GMV in the left cerebellum of the WMH group was reduced when compared to the control group. The cerebellum is an important regulatory center of movement, with a large number of incoming and outgoing connections. Also, it plays an important role in maintaining body balance receives information from the vestibular organs, and changes the tension of muscles in different parts of the body through outgoing connections, so that the body maintains a balanced posture during acceleration or rotation under the action of gravity. Importantly, it plays an important role in vision. Thus, any damage to this structure can lead to damage to the sensory system and gait disturbances, as previously reported [29,30]. Here we suggest that these GMV differences seen between older adults with WMH and controls may reflect the widespread degeneration.

We also showed GMV was lower in the left frontal inferior orbital gyrus and left frontal middle orbital gyrus of older adults with WMH when compared with the control group; moreover, an association was shown between the RNFL thickness and the left frontal inferior orbital gyrus and left frontal middle orbital gyrus respectively in older adults with WMH. The left frontal inferior orbital and left frontal middle orbital gyrus are part of the orbitofrontal cortex, which sits above the orbits. The orbitofrontal cortex has extensive connections with sensory areas as well as limbic system structures involved in emotion and memory. A previous report [31] showed that cerebral small vessel disease patients with gait impairments have significantly reduced orbitofrontal cortical thickness. Our current report suggests that changes in the orbitofrontal cortex occur during the subclinical phase of neurodegenerative disease; the association between these cerebral structures and the RNFL suggests that changes in these cerebral structures may reflect the changes in the eye echoing the association between the brain and the eye.

Reduced FA occurs in WMH and indicates sub-visible alterations in the axonal integrity, fiber density, or myelin structure [32]. Here we found that thinner peripapillary RNFL thickness in older adults with WMH was associated with sub-visible white matter damage (reduced FA in the superior longitudinal fasciculus and splenium of corpus callosum) in keeping with increased demyelination and axonal loss [33,34]. It will be important to assess whether early retinal structural changes can predict WMH progression and white matter damage in the long term.

WMH is a common characteristic of SVD on brain MRI. Previous studies used the Fazekas score to represent WMH severity and showed retinal structural thicknesses correlated with increased Fazekas score [12,16]. Here, worse WMH scores (assessed by visual rating) correlated with thinner peripapillary RNFL thickness in older adults with WMH.

Pivotal methodologies for diagnosis of cognitive functioning are based on neuropsychological assessments such as mini-mental state examination scores (MMSE) [35]. In our current study, we found a significant association between the MMSE score and the RNFL which is congruent with previous reports [11,27]. An association between the RNFL and MMSE scores suggests that the neurodegeneration associated with the WMH causes neuro-axonal damage resulting in the decline of cognitive functioning.

An important aspect of this study was a comprehensive brain imaging protocol that produced key metrics about the brain. We would like to acknowledge some limitations in our study. To begin with, the observational cross-sectional design of our study confines us to draw assumptions about the cause and effect; longitudinal studies with larger sample sizes are needed to investigate more on our current study and validate our hypotheses. As with most diagnostic tests, patient cooperation is an obligation. Head and/or eye movement from the participant can diminish the quality of the image and some participants were excluded from the study because of eye movement during the examination as such some images were excluded due to poor imaging which may introduce bias. This is important in clinical studies that are more likely exhibit movement compromising the quality of the data. Before actual scanning, study participants can be trained on a mock scanner to mitigate this issue. Movement can also be accounted for in the analysis phase. There are several pitfalls to TBSS, including the inability to correct misalignment and a lack of sensitivity and specificity. As in most previous studies, differences in white matter were observed in the corpus callosum and other large matter pathways. DTI has problems with kissing and crossing fibers. In neural areas with multiple fiber paths crossing, this model has difficulty modeling them accurately. Consideration should be given to techniques more robust to such intersection such as high angular diffusion magnetic imaging (HARDI) or diffusion spectral imaging (DSI). Another limitation of our study is the lack of evaluation of other layers of the retina structures; however, we used the OCT machine to evaluate the peripapillary RNFL. Reports with a segmentation algorithm of the retina are needed to elucidate the association between the macular thickness and cerebral metrics.

5. Conclusions

In conclusion, we showed neurodegeneration of peripapillary RNFL changes in older adults with WMH were associated with cerebral microstructural volume, impaired cerebral axonal damage, and cognitive performances. Our current report suggests that OCT measures hold promise to reflect neurodegenerative processes in WMH that may subsequently progress to a clinically apparent phase.

Availability of Data and Materials

The datasets used and analyzed during the current study are available from the corresponding author on reasonable request.

Author Contributions

ZH, YW and JY designed the research study. YW and JY performed the research. ZH and YC provided help and advice on resources and data interpretation. YW, JY, LX, CX, MZ, ZZ, YL and XL analyzed the data. YW and JY wrote the manuscript. All authors contributed to editorial changes in the manuscript. All authors read and approved the final manuscript. All authors have participated sufficiently in the work and agreed to be accountable for all aspects of the work.

Ethics Approval and Consent to Participate

The studies involving human participants were approved by the Ethics Committee of the Second Affiliated Hospital and Yuying Children's Hospital of Wenzhou Medical University (Ethics Approval No. 10 [2017], Clinical Science Review) and written informed consent was obtained from each participant. All subjects were treated following the tenets of the Declaration of Helsinki.

Acknowledgment

Not applicable.

Funding

This study was funded by Clinical Scientific Research Fund of the Second Affiliated Hospital of Wenzhou Medical University [SAHoWMU-CR2017-01-212], the National Natural Science Foundation of China (Grant no. 82271344, 81771267).

Conflict of Interest

The authors declare no conflict of interest.

Supplementary Material

Supplementary material associated with this article can be found, in the online version, at <https://doi.org/10.31083/j.jin2303056>.

References

- [1] Alber J, Alladi S, Bae HJ, Barton DA, Beckett LA, Bell JM, *et al.* White matter hyperintensities in vascular contributions to cognitive impairment and dementia (VCID): Knowledge gaps and opportunities. *Alzheimer's & Dementia (New York, N. Y.)*. 2019; 5: 107–117.
- [2] van den Berg E, Geerlings MI, Biessels GJ, Nederkoorn PJ, Kloppenborg RP. White Matter Hyperintensities and Cognition in Mild Cognitive Impairment and Alzheimer's Disease: A Domain-Specific Meta-Analysis. *Journal of Alzheimer's Disease: JAD*. 2018; 63: 515–527.
- [3] Moroni F, Ammirati E, Hainsworth AH, Camici PG. Association of White Matter Hyperintensities and Cardiovascular Disease: The Importance of Microcirculatory Disease. *Circulation. Cardiovascular Imaging*. 2020; 13: e010460.
- [4] Pfitzner M, Bleau M, Bouskila J. The Retina: A Window into the Brain. *Cells*. 2021; 10: 3269.
- [5] Mutlu U, Bonnemaier PWM, Ikram MA, Colijn JM, Cremers LGM, Buitendijk GHS, *et al.* Retinal neurodegeneration and brain MRI markers: the Rotterdam Study. *Neurobiology of Aging*. 2017; 60: 183–191.
- [6] Lima Rebouças SC, Crivello F, Tsuchida A, Tzourio C, Schweitzer C, Korobelnik JF, *et al.* Association of retinal nerve layers thickness and brain imaging in healthy young subjects from the i-Share-Bordeaux study. *Human Brain Mapping*. 2023; 44: 4722–4737.
- [7] Peng C, Kwapong WR, Shasha X, Farah MM, Jueyan Y, Qu M, *et al.* Structural and Microvascular Changes in the Macular Area Associated With Severity of White Matter Lesions. *Frontiers in Neurology*. 2020; 11: 521.
- [8] Thomson KL, Yeo JM, Waddell B, Cameron JR, Pal S. A systematic review and meta-analysis of retinal nerve fiber layer change in dementia, using optical coherence tomography. *Alzheimer's & Dementia (Amsterdam, Netherlands)*. 2015; 1: 136–143.
- [9] Kim HM, Han JW, Park YJ, Bae JB, Woo SJ, Kim KW. Association Between Retinal Layer Thickness and Cognitive Decline in Older Adults. *JAMA Ophthalmology*. 2022; 140: 683–690.
- [10] Ko F, Muthy ZA, Gallacher J, Sudlow C, Rees G, Yang Q, *et al.* Association of Retinal Nerve Fiber Layer Thinning With Current and Future Cognitive Decline: A Study Using Optical Coherence Tomography. *JAMA Neurology*. 2018; 75: 1198–1205.
- [11] Girbardt J, Luck T, Kynast J, Rodriguez FS, Wicklein B, Wirkner K, *et al.* Reading cognition from the eyes: association of retinal nerve fibre layer thickness with cognitive performance in a population-based study. *Brain Communications*. 2021; 3: fcb258.
- [12] Peng C, Kwapong WR, Xu S, Muse FM, Yan J, Qu M, *et al.* Structural and Microvascular Changes in the Macular Area Associated With Severity of White Matter Lesions. *Frontiers in Neurology*. 2020; 11: 521.
- [13] Ong YT, Hilal S, Cheung CY, Venketasubramanian N, Niessen WJ, Vrooman H, *et al.* Retinal neurodegeneration on optical coherence tomography and cerebral atrophy. *Neuroscience Letters*. 2015; 584: 12–16.
- [14] Chanraud S, Zahr N, Sullivan EV, Pfefferbaum A. MR diffusion tensor imaging: a window into white matter integrity of the working brain. *Neuropsychology Review*. 2010; 20: 209–225.
- [15] Mei Y, Wang W, Qiu D, Yuan Z, Bai X, Tang H, *et al.* Microstructural white matter abnormalities in new daily persistent headache: a DTI study using TBSS analysis. *The Journal of Headache and Pain*. 2023; 24: 80.
- [16] Qu M, Kwapong WR, Peng C, Cao Y, Lu F, Shen M, *et al.* Retinal sublayer defect is independently associated with the severity of hypertensive white matter hyperintensity. *Brain and Behavior*. 2020; 10: e01521.
- [17] Fazekas F, Chawluk JB, Alavi A, Hurtig HI, Zimmerman RA. MR signal abnormalities at 1.5 T in Alzheimer's dementia and normal aging. *AJR. American Journal of Roentgenology*. 1987; 149: 351–356.
- [18] Nichols TE, Holmes AP. Nonparametric permutation tests for functional neuroimaging: a primer with examples. *Human Brain Mapping*. 2002; 15: 1–25.
- [19] Rolls ET, Joliot M, Tzourio-Mazoyer N. Implementation of a new parcellation of the orbitofrontal cortex in the automated anatomical labeling atlas. *NeuroImage*. 2015; 122: 1–5.
- [20] Hua K, Zhang J, Wakana S, Jiang H, Li X, Reich DS, *et al.* Tract probability maps in stereotaxic spaces: analyses of white matter anatomy and tract-specific quantification. *NeuroImage*. 2008; 39: 336–347.

- [21] Tewarie P, Balk L, Costello F, Green A, Martin R, Schippling S, *et al.* The OSCAR-IB consensus criteria for retinal OCT quality assessment. *PloS One*. 2012; 7: e34823.
- [22] Aytulun A, Cruz-Herranz A, Aktas O, Balcer LJ, Balk L, Barboni P, *et al.* APOSTEL 2.0 Recommendations for Reporting Quantitative Optical Coherence Tomography Studies. *Neurology*. 2021; 97: 68–79.
- [23] Smith SM, Nichols TE. Threshold-free cluster enhancement: addressing problems of smoothing, threshold dependence and localisation in cluster inference. *NeuroImage*. 2009; 44: 83–98.
- [24] Kwapong WR, Gao Y, Yan Y, Zhang Y, Zhang M, Wu B. Assessment of the outer retina and choroid in white matter lesions participants using swept-source optical coherence tomography. *Brain and Behavior*. 2021; 11: e2240.
- [25] Lv X, Teng Z, Jia Z, Dong Y, Xu J, Lv P. Retinal thickness changes in different subfields reflect the volume change of cerebral white matter hyperintensity. *Frontiers in Neurology*. 2022; 13: 1014359.
- [26] Chua SYL, Lascaratos G, Atan D, Zhang B, Reisman C, Khaw PT, *et al.* Relationships between retinal layer thickness and brain volumes in the UK Biobank cohort. *European Journal of Neurology*. 2021; 28: 1490–1498.
- [27] Wang R, Kwapong WR, Tao W, Cao L, Ye C, Liu J, *et al.* Association of retinal thickness and microvasculature with cognitive performance and brain volumes in elderly adults. *Frontiers in Aging Neuroscience*. 2022; 14: 1010548.
- [28] Barrett-Young A, Abraham WC, Cheung CY, Gale J, Hogan S, Ireland D, *et al.* Associations Between Thinner Retinal Neuronal Layers and Suboptimal Brain Structural Integrity in a Middle-Aged Cohort. *Eye and Brain*. 2023; 15: 25–35.
- [29] Ter Telgte A, van Leijssen EMC, Wiegertjes K, Klijn CJM, Tulladhar AM, de Leeuw FE. Cerebral small vessel disease: from a focal to a global perspective. *Nature Reviews. Neurology*. 2018; 14: 387–398.
- [30] Yeo JK, Hun KK, Jong ML, Hanna C, Hee JK, Hee KP, *et al.* Gray and white matter changes linking cerebral small vessel disease to gait disturbances. *Neurology*. 2016; 86: 1199–1207.
- [31] de Laat KF, Reid AT, Grim DC, Evans AC, Kötter R, van Norden AGW, *et al.* Cortical thickness is associated with gait disturbances in cerebral small vessel disease. *NeuroImage*. 2012; 59: 1478–1484.
- [32] Veeramuthu V, Narayanan V, Kuo TL, Delano-Wood L, Chinna K, Bondi MW, *et al.* Diffusion Tensor Imaging Parameters in Mild Traumatic Brain Injury and Its Correlation with Early Neuropsychological Impairment: A Longitudinal Study. *Journal of Neurotrauma*. 2015; 32: 1497–1509.
- [33] van Leijssen EMC, Bergkamp MI, van Uden IWM, Ghafoorian M, van der Holst HM, Norris DG, *et al.* Progression of White Matter Hyperintensities Preceded by Heterogeneous Decline of Microstructural Integrity. *Stroke*. 2018; 49: 1386–1393.
- [34] Kuang Q, Huang M, Lei Y, Wu L, Jin C, Dai J, *et al.* Clinical and cognitive correlates tractography analysis in patients with white matter hyperintensity of vascular origin. *Frontiers in Neuroscience*. 2023; 17: 1187979.
- [35] McKhann G, Drachman D, Folstein M, Katzman R, Price D, Stadlan EM. Clinical diagnosis of Alzheimer's disease: report of the NINCDS-ADRDA Work Group under the auspices of Department of Health and Human Services Task Force on Alzheimer's Disease. *Neurology*. 1984; 34: 939–944.